32

Hydraulic Tomography

Deqiang Mao
Colorado School of Mines

Tian-Chyi J. Yeh
University of Arizona

Walter Illman
University of Waterloo

André Revil
University Savoie Mont Blanc ISTerre, CNRS

Jet-Chau Wen
National Yunlin University of Science and Technology

Yuanyuan Zha
Wuhan University

32.1 Introduction 897
32.2 Governing Equations 898
Governing Equation for Steady-State Flow in Confined Aquifers • Governing Equation for Transient-State Flow in Confined Aquifers • Governing Equation for Transient-State Flow in Unconfined Aquifers
32.3 Stochastic Representation of Heterogeneity 899
32.4 Cross-Correlation between Head Measurements and Parameter Fields 900
2-D Confined Aquifer Example • 3-D Unconfined Aquifer Example
32.5 Successive Linear Estimator 904
Steady-State Flow in Confined Aquifers • Transient-State Flow in Confined Aquifers • Transient-State Flow in Unconfined Aquifers
32.6 Adjoint-State Method 907
32.7 Strategy for Implementation of HT Tests 908
32.8 Examples of HT Tests 908
Sequential Tomographic Test under Steady-State Conditions • Transient Hydraulic Tomography in Fracture Geologic Media • Hydraulic Tomography Test in a Controlled Sandbox
32.9 Tomographic Tests in Geophysics 912
32.10 Summary 912
Glossary 912
References 914
Further Information 916

32.1 Introduction

Hydrologic properties of geologic media always exhibit a high degree of spatial variability at various scales due to the heterogeneous nature of geologic formations. Detailed characterization of inherent aquifer heterogeneity is necessary for an accurate assessment of groundwater resources and pollution problems.

Traditional characterization approaches have adopted homogeneous conceptual models that assume aquifer homogeneity and have attempted to derive effective hydraulic parameters based on drawdowns from a single pumping test, for example, those by Theis (1935) and Cooper and Jacob (1946) for confined aquifers and those by Boulton (1963), Dagan (1967), Streltsova (1976a,b), Neuman (1972), Moench (1995), Mathias and Butler (2006), and Mishra and Neuman (2010) for unconfined aquifers. Type curve methods are often employed to obtain an effective homogeneous parameter (see Chapter 29). Wu et al. (2005), Straface et al. (2007), and Huang et al. (2011) challenged these traditional aquifer test methods.

Geostatistical method permits investigators to interpolate and extrapolate hydraulic parameters derived from core samples, or pumping tests from several boreholes in the field to estimate the spatial distribution of hydraulic parameters over a large domain. It can preserve the sample values at sampling locations, and it estimates parameter values at locations where samples are not available based on spatial statistics to derive statistically unbiased estimates. The accuracy of these estimates relies on the density of spatial samples and representativeness of the samples. For most field problems, the density of samples is sparse and the estimates are of great uncertainty (Ni et al., 2009).

While the concept of hydraulic tomography (HT) has been proposed by many in the past, the pioneering development of 3-D HT technology for mapping 3-D hydraulic heterogeneity by Yeh and Liu (2000) and Zhu and Yeh (2005) has motivated many researchers to investigate the potentials for characterizing the spatial distributions of hydraulic parameters using HT during the past decade. HT is merely a sequential pumping test or multi-well interference test. Specifically, an aquifer is stressed by

pumping water from or injecting water into a well (or a location of an aquifer), and the responses of the aquifer are monitored at other wells (locations). Sequentially switching the pumping or injection locations, without installing additional wells, results in a large number of aquifer responses induced by stresses at different locations. Each set of stress/responses data is tantamount to a snapshot of the aquifer heterogeneity at a different location (or angle and perspective), carrying nonredundant information about aquifer heterogeneity. A joint interpretation of these nonredundant datasets therefore makes HT possible to characterize aquifer with high resolution.

We categorize the past HT research works into three categories: numerical studies, sandbox investigations, and field verifications. The numerical studies include works by Yeh and Liu (2000), Vasco and Karasaki (2001), Bohling et al. (2002), Zhu and Yeh (2005), Fienen et al. (2008), Ni and Yeh (2008), Castagna and Bellin (2009), Xiang et al. (2009), Liu and Kitanidis (2011), Cardiff and Barrash (2011), Cardiff et al. (2013), Mao et al. (2013b), and Zha et al. (2014). Meanwhile, some researchers have conducted sandbox experiments to test and verify the potential of using laboratory experiments, for example, Liu et al. (2002, 2007), Brauchler et al. (2003, 2013), Illman et al. (2007, 2010, 2012), Yin and Illman (2009), and Zhao et al. (2015). Moreover, field experiments have also been conducted to test the ability of HT, for example, Bohling et al. (2007), Li et al. (2007), Straface et al. (2007), Cardiff and Barrash (2011), Illman et al. (2009), Berg and Illman (2011a,b), Brauchler et al. (2011), and Huang et al. (2011).

Over the past decade, these studies have consistently shown that HT can identify not only the pattern of the heterogeneous hydraulic conductivity field but also the variation of specific storage, as well as unsaturated parameters. More importantly, they have demonstrated that the hydraulic property fields estimated by HT can yield much better predictions of flow and transport processes than conventional characterization approaches (e.g., Liu et al., 2007; Xiang et al., 2009; Berg and Illman, 2011b; Illman et al., 2012). More recently, Hao et al. (2008), Illman et al. (2009), and Sharmeen et al. (2012) have also demonstrated the success of HT for characterizing fracture connectivity.

As HT has been proven as a matured new technology for aquifer characterization over the past decade, it is the intention of this chapter to provide an introduction to this matured technology to groundwater hydrologists and engineers for its broader applications. As a result, in this chapter, we first discuss the governing flow equations, and then stochastic conceptualization of the parameters in the equations. Afterward, we introduce cross-correlation analysis to explain the information content of observed heads at a sample location about hydraulic parameters everywhere in confined and unconfined aquifers. Based on the results of the cross-correlation analysis, the rationale behind the HT is elucidated. We subsequently discuss the key algorithm for HT analysis (i.e., successive linear estimator [SLE]) for steady- and transient-state flow in confined and unconfined aquifers. Then, we discuss a strategy for implementation of HT analysis and three HT examples. At last, some extended applications in geophysics are introduced.

32.2 Governing Equations

Flow of groundwater is governed by differential equations under various conditions. We first introduce different flow regimes and the corresponding governing equations.

32.2.1 Governing Equation for Steady-State Flow in Confined Aquifers

For 3-D groundwater flow under steady-state condition in heterogeneous porous media, flow can be described by the following equation and boundary conditions:

$$\begin{aligned} &\nabla \cdot \left[K(\mathbf{x})\nabla\phi\right] + Q(\mathbf{x}_p) = 0 \\ &\phi|_{\Gamma_1} = \phi^* \\ &\left[K(\mathbf{x})\nabla\phi\right]\cdot\mathbf{n}|_{\Gamma 2} = q \end{aligned} \tag{32.1}$$

where

∇ is the differential operator
ϕ is total head (m)
$\mathbf{x}$ is the spatial coordinate ($\mathbf{x} = \{x, y, z\}$, [m]), and z represents the vertical coordinate and is positive upward
Q is the pumping rate (1/s) at the selected interval during the tomography experiment
$K(\mathbf{x})$ is the saturated hydraulic conductivity field (m/s)

Prescribed total head on the Dirichlet boundary Γ_1 is denoted by ϕ^* (m) and the Neumann boundary Γ_2 condition has specified flux q (m/s), and $\mathbf{n}$ is a unit vector normal to the boundary.

32.2.2 Governing Equation for Transient-State Flow in Confined Aquifers

Under transient condition, the change of the elastic storage of the aquifer should be considered, and the governing equation under transient-state condition in heterogeneous porous media becomes

$$\begin{aligned} &\nabla \cdot \left[K(\mathbf{x})\nabla\phi\right] + Q(\mathbf{x}_p) = S_s(\mathbf{x})\frac{\partial\phi}{\partial t} \\ &\phi|_{\Gamma_1} = \phi^* \\ &\left[K(\mathbf{x})\nabla\phi\right]\cdot\mathbf{n}|_{\Gamma 2} = q \\ &\phi|_{t=0} = \phi_0 \end{aligned} \tag{32.2}$$

where $S_s(\mathbf{x})$ is the heterogeneous specific storage (1/m) and the flow domain is prescribed with an initial condition ϕ_0. The other conditions are similar to the steady-state condition.

32.2.3 Governing Equation for Transient-State Flow in Unconfined Aquifers

With the inclusion of unsaturated flow in unconfined aquifers, we chose variably saturated flow equation as a suitable candidate to describe it:

$$\begin{aligned}
&\nabla\cdot\left[K(\varphi,\mathbf{x})\nabla(\varphi+z)\right]+Q(\mathbf{x}_p)=\left[\omega S_s(\mathbf{x})+C(\varphi,\mathbf{x})\right]\frac{\partial\varphi}{\partial t}\\
&\varphi|_{\Gamma_1}=\varphi^*\\
&\left[K(\varphi,\mathbf{x})\nabla(\varphi+z)\right]\cdot\mathbf{n}|_{\Gamma_2}=q\\
&\varphi|_{t=0}=\varphi_0
\end{aligned}\tag{32.3}$$

Often, pressure head φ is used in the governing equation rather than total head ϕ to emphasize the pressure-dependent hydraulic parameters. The saturation index ω is equal to one if the medium is saturated and zero if the medium is unsaturated. $\theta(\varphi, \mathbf{x})$ represents the volumetric moisture content, $C(\varphi, \mathbf{x})=d\theta(\varphi, \mathbf{x})/d\psi$ (1/m) is the soil moisture capacity, and $K(\varphi, \mathbf{x})$ is the unsaturated hydraulic conductivity. Both conductivity and water content become pressure dependent.

The van Genuchten model (1980) is often used to describe the pressure-dependent water content:

$$\theta(\varphi,\mathbf{x})=\theta_r(\mathbf{x})+\frac{\theta_s(\mathbf{x})-\theta_r(\mathbf{x})}{\left[1+\left|\alpha(\mathbf{x})\varphi(\mathbf{x})\right|^n\right]^m}\tag{32.4}$$

where θ_r and θ_s are the residual and saturated moisture content. The parameter α is related to the inverse of the air entry suction (1/m). n is a measure of the pore size distribution and $m=1-1/n$. Location vector $\mathbf{x}$ is added in each parameter of Equation 32.4 to emphasize the heterogeneous distribution. The corresponding hydraulic conductivity is derived by Mualem (1976) and it is often expressed with the effective saturation S_e as a variable

$$K(S_e)=K_s(\mathbf{x})S_e^L\left[1-(1-S_e^{1/m})^m\right]^2\tag{32.5}$$

where L is an empirical pore connectivity parameter, and 0.5 is often selected. The expression for effective saturation is

$$S_e(\mathbf{x})=\frac{\theta(\varphi,\mathbf{x})-\theta_r(\mathbf{x})}{\theta_s(\mathbf{x})-\theta_r(\mathbf{x})}\tag{32.6}$$

Equations 32.4 through 32.6 describe the pressure-dependent parameters precisely. However, it brings convergence problem during parameter estimation process. Therefore, some simplified models are often used instead. Gardner (1958) and Russo (1988) models are often used. The following two equations describe the pressure-dependent hydraulic conductivity and moisture content:

$$K(\varphi,\mathbf{x})=K_s(\mathbf{x})e^{\alpha(\mathbf{x})\varphi}\tag{32.7}$$

$$\theta(\varphi,\mathbf{x})=\theta_r+(\theta_s-\theta_r)\left\{e^{0.5\alpha(\mathbf{x})\varphi}\left[1-0.5\alpha(\mathbf{x})\varphi\right]\right\}^{2/2+m}\tag{32.8}$$

where m is related to the tortuosity of the soil and is often assumed to be zero for simplicity and a is the parameter related to pore size distribution.

32.3 Stochastic Representation of Heterogeneity

For the application of HT concept, most of the existing methods rely on the stochastic representation of heterogeneity. To describe the spatial variability of the hydraulic conductivity, $K(\mathbf{x})$, we normally use the natural logarithm values $\ln K(\mathbf{x})$ as the variables not only because it is generally found to have a log normal distribution (Sudicky, 1986), but also it could avoid negative values in generating random fields. Based on stationary assumption, $\ln K(\mathbf{x})$ can be processed as

$$\ln K(\mathbf{x})=Y=\overline{f}+f(\mathbf{x})\tag{32.9}$$

where

vector $\mathbf{x}$ represents the spatial location
$\overline{f}$ denotes the mean of $\ln K(\mathbf{x})$, which is constant in space
$f(\mathbf{x})$ is the perturbation (or random part) about the mean

To describe the spatial variability of the process, we then specify its mean, variance, and autocovariance:

$$\text{Mean } E[\ln K(\mathbf{x})]=\overline{f}\tag{32.10}$$

$$\text{Variance } \sigma_f^2=E\left[(\ln K(\mathbf{x})-\overline{f})^2\right]\tag{32.11}$$

$$\text{Autocovariance function } C(\xi)=\sigma_f^2\exp\left(-\frac{|\xi|}{\lambda}\right)\tag{32.12}$$

Here we use a 3-D isotropic stochastic process as an example, where ξ is the distance between two spatial points and λ is the isotropic correlation scale. Of course, variogram can be used to replace the covariance function. Variogram could be obtained with less stringent intrinsic hypothesis than the second-order stationary used for autocovariance (see Chapter 34 for details).

With the same stochastic assumption, the logarithm of other hydraulic parameters could be treated with a mean and a perturbation:

$$\ln S_s(\mathbf{x})=\overline{s}+s(\mathbf{x});\quad \ln\alpha(\mathbf{x})=\overline{a}+a(\mathbf{x});\quad \ln\theta_s(\mathbf{x})=\overline{t}_s+t_s(\mathbf{x})\tag{32.13}$$

At the same time, the corresponding hydraulic head can also be represented in this manner:

$$\phi=\overline{H}(\mathbf{x})+h(\mathbf{x})\tag{32.14}$$

where
$\bar{H}(\mathbf{x})$ is the mean hydraulic head
$h(\mathbf{x})$ is the head perturbation

With the aforementioned stochastic representations for hydraulic parameters and the corresponding head response incorporation into groundwater governing equations, and combined with cokriging geostatistical method, HT methods could be implemented.

32.4 Cross-Correlation between Head Measurements and Parameter Fields

During HT parameter estimation, head observations from different pumping tests are analyzed together to obtain a high resolution characterization. The rationality behind this is that different observation datasets reflect the heterogeneity in different regions of an aquifer. Cross-correlation analysis can be utilized to show information content for each observation data. We advocate the use of cross-correlation rather than sensitivity for evaluating the information content in each observation data (see discussion in Mao et al., 2013a).

> The cross-correlation analysis is a sensitivity analysis casted in a stochastic framework. It employs the stochastic or geostatistic concept. It includes not only the variance of the parameter but also the spatial covariance function or variogram of the parameter to depict how an observed head is influenced by unknown spatial variability of parameters. Physically, the variogram represents the average dimensions of "geofabrics" (i.e., layers, stratifications, or structures) in the aquifer. The cross-correlation analysis therefore considers not only the governing flow equation and the most likely value of hydraulic properties (as in sensitivity analysis), but also the possible magnitude of heterogeneity (variance) and the geologic fabrics of an aquifer to investigate how the head at $(\mathbf{x}_i, t)$ is affected by the heterogeneity in every part of the aquifer.

We introduce the definition of cross-correlation between head measurements and parameter fields. In the stochastic frame work, head covariance from the effect of variability of all the parameter could be approximated as

$$\mathbf{R}_{hh} = \mathbf{J}_f \mathbf{R}_{ff} \mathbf{J}_f^T + \mathbf{J}_s \mathbf{R}_{ss} \mathbf{J}_s^T + \mathbf{J}_a \mathbf{R}_{aa} \mathbf{J}_a^T + \mathbf{J}_{t_s} \mathbf{R}_{t_s t_s} \mathbf{J}_{t_s}^T \quad (32.15)$$

where the superscript T denotes the transpose. The diagonal components of $\mathbf{R}_{hh}$ are head variances $\sigma_h^2(\mathbf{x}_i,t)$. The symbols are slightly different from Equation 32.30 to emphasize that the variances of all parameters are evaluated at the start of an inversion process $\mathbf{R}$, not residual variance ε. Detailed derivation of the cross-correlation for each parameter will be discussed in Section 32.5. We present the cross-correlation for all the parameters directly:

$$\rho_{hf}(\mathbf{x}_i,t) = \frac{\mathbf{J}_{hf}(t)\mathbf{R}_{ff}}{\sqrt{\sigma_h^2(\mathbf{x}_i,t)\sigma_f^2}} \quad \rho_{hs}(\mathbf{x}_i,t) = \frac{\mathbf{J}_{hs}(t)\mathbf{R}_{ss}}{\sqrt{\sigma_h^2(\mathbf{x}_i,t)\sigma_s^2}}$$
$$\rho_{ha}(\mathbf{x}_i,t) = \frac{\mathbf{J}_{ha}(t)\mathbf{R}_{aa}}{\sqrt{\sigma_h^2(\mathbf{x}_i,t)\sigma_a^2}} \quad \rho_{hts}(\mathbf{x}_i,t) = \frac{\mathbf{J}_{ht_s}(t)\mathbf{R}_{t_s t_s}}{\sqrt{\sigma_h^2(\mathbf{x}_i,t)\sigma_{t_s}^2}} \quad (32.16)$$

where $\boldsymbol{\rho}_{hf}$, $\boldsymbol{\rho}_{hs}$, $\boldsymbol{\rho}_{ha}$, and $\boldsymbol{\rho}_{hts}$ are the cross-correlation matrix between observed heads and hydraulic conductivity, specific storage, pore size distribution parameter a, and saturated water content, which usually are the unknown parameters during an inverse problem. $\sigma_h^2(\mathbf{x}_i,t)$ is the head variance, which represent the uncertainty in head at $(\mathbf{x}_i, t)$, and σ_f^2 is the variance of hydraulic conductivity.

The cross-correlation matrices represents the relation between head at $(\mathbf{x}_i, t)$ and hydraulic conductivity at each of the N discretized elements in the domain, which is normalized by the square root of the product of the variances of h at $(\mathbf{x}_i, t)$ and the corresponding variance of the parameter. This cross-correlation could be used to evaluate the information content embedded in the head measurements. We use two published results by Sun et al. (2013) and Mao et al. (2013a) to illustrate its performance under different conditions.

32.4.1 2-D Confined Aquifer Example

Sun et al. (2013) employed cross-correlation analysis to obtain the temporal sampling strategy for transient HT analysis. They use a 2-D confined aquifer to show the variation of cross-correlation between observation heads and logarithm of transmissivity T and storativity S (which is defined by multiplying the thickness of an aquifer with K_s and S_s). The numerical analysis was conducted in a 200 m × 200 m aquifer surrounded by 100 m constant head boundary. The pumping well is located at x = 120 m, y = 100 m, and an observation well was at x = 80 m, y = 100 m.

At the early stage of the pumping test t = 200 s, cross-correlation ρ_{hy} (it is similar to ρ_{hf}) between head and ln T has negative values over a large area and with the highest correlation −0.6 in the region between pumping well and observation well (Figure 32.1a). At the same time, cross-correlation ρ_{hz} (it is similar to ρ_{hs}) between head and ln S has a range from 0.1 to 0.4 (Figure 32.1b). The highest values are also confined to a small region between the pumping well and observation well. At this very early time, the cone of depression is restricted to a very small area. Therefore, those high cross-correlation values is not useful to estimate hydraulic properties at the observation well and beyond.

With continued pumping, noticeable drawdown has expanded to the observation well (Figure 32.1c and d) at t = 1100 s. ρ_{hy} has high negative values range from −0.5 to 0 in the region between pumping well and observation well. The negative correlation means that if the observation head in a heterogeneous aquifer is higher than the head calculated from the mean values of the aquifer, the T values downstream of the observation are likely to be lower than the mean T value. During this same period, ρ_{hz} value has a range from 0.1 to 0.4 with its highest value located in a

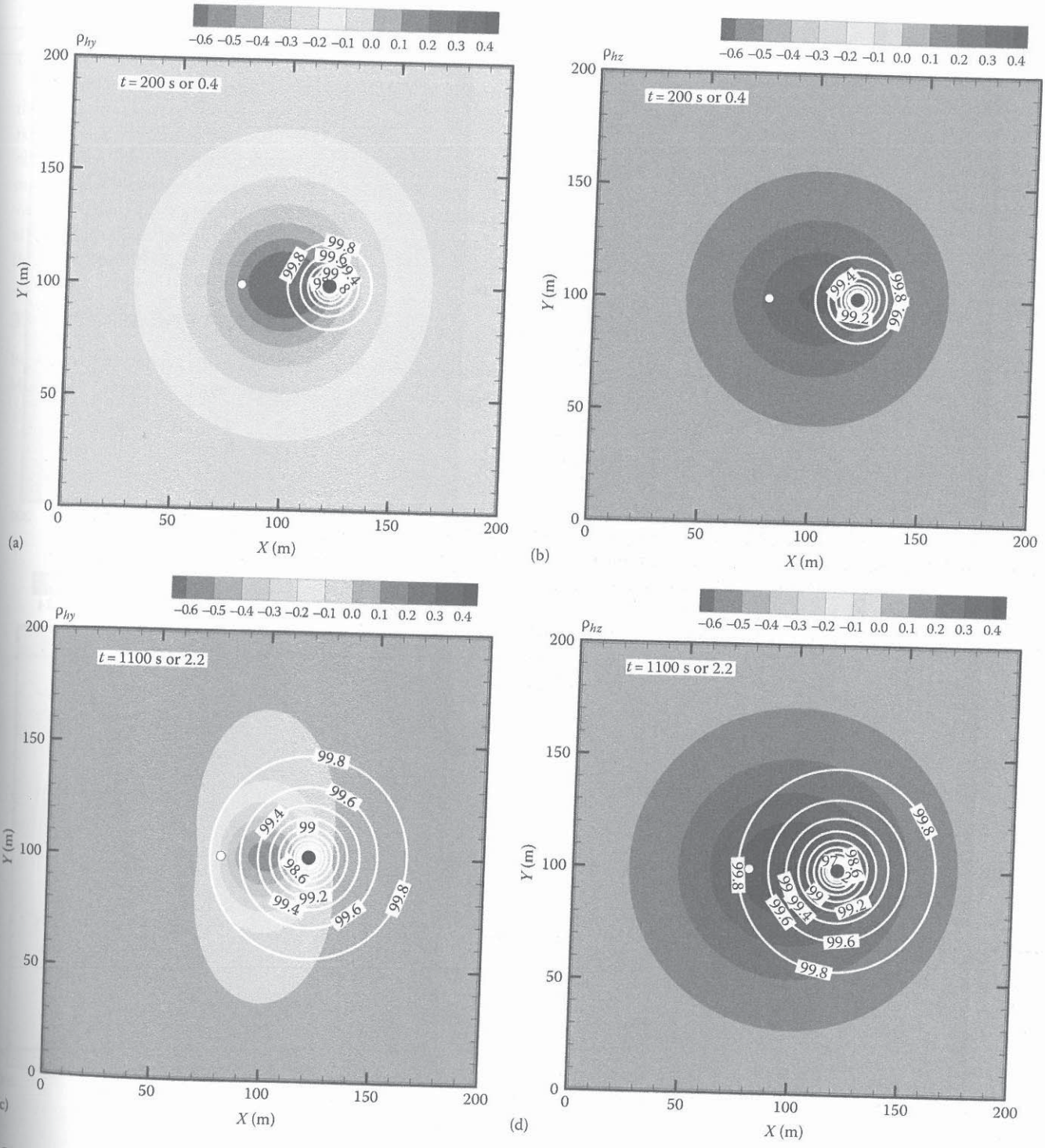

FIGURE 32.1 Contour map of cross-correlation between observation head (white circle) and ln T (a and c) and ln S (b and d) in the aquifer at early time 200 and 1100 s after pumping started at the pumping well (black circle). White contours are equipotential lines. (From Sun, R. et al., *Water Resour. Res.*, 49, 3881, 2013, Figure 2.)

circular area between the pumping well and observation well. A positive correlation implies that if an observation head is higher than the head calculated from the mean values, the S values in the positive area are likely to be higher than the mean S value. At this period, the area covered by significant ρ_{hz} values is much larger than that of ρ_{hy}. This means that observation head is highly influenced by the S heterogeneity in the small red region with $\rho_{hz} = 0.4$.

At intermediate time $t = 3000$ (Figure 32.2a and b), the cone of depression has reached to the right-hand side of the boundary. ρ_{hz} has similar pattern with the period at $t = 1100$ s but the value

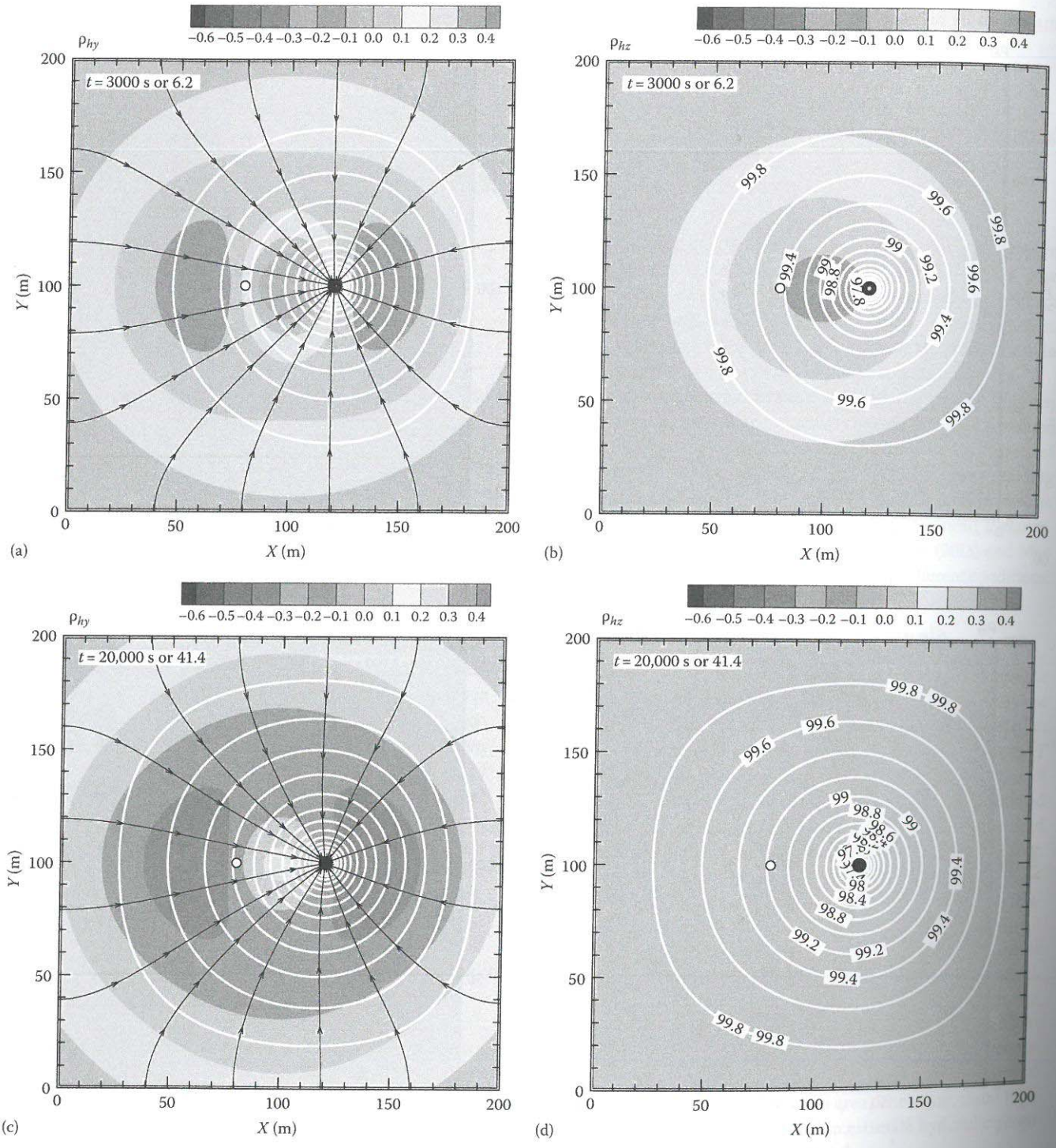

FIGURE 32.2 Contour map of cross-correlation between observation head (white circle) and ln T (a and c) and ln S (b and d) in the aquifer at early time 3,000 and 20,000 s after pumping started at the pumping well (black circle). White contours are equipotential lines. (From Sun, R. et al., *Water Resour. Res.*, 49, 3881, 2013, Figure 3.)

drops below 0.4 (Figure 32.2b), indicating the effect of storage is diminishing and flow is moving toward a steady state. At this time, $\boldsymbol{\rho}_{hy}$ has become positive everywhere in the aquifer. There are two kidney-shaped humps formed at upstream of the observation and at the upstream of the pumping well.

When the flow reaches steady state at $t = 20{,}000$ s, the pattern of $\boldsymbol{\rho}_{hy}$ is similar to that at $t = 3{,}000$ s but their magnitude everywhere are elevated (Figure 32.2c). Meanwhile, $\boldsymbol{\rho}_{hz}$ values diminish to zero everywhere to show that the steady hydraulic head is not related to S (Figure 32.2d). The two kidney-shaped spatial

pattern of the cross-correlation between ln T and the head is different from the sensitivity behavior based on radial symmetric flow model used by Bohling et al. (2007).

These spatial patterns of the cross-correlation analysis from the 2-D example provide us some insight for parameters with respect to S and T. The high values ρ_{hz} at early time tell us that observation from this period is good for S estimation; however, it only gives information for area between pumping well and observation well. ρ_{hy} has high values over the entire cone of depression at late time or steady state. Therefore, adding new head data from this period will bring more information about T heterogeneity.

32.4.2 3-D Unconfined Aquifer Example

Besides the aforementioned 2-D example in confined aquifers, Mao et al. (2013a) conducted a cross-correlation analysis for all the hydraulic parameters involved in a 3-D unconfined aquifer, where the pumping well is located at $x = 100$ m, $y = 100$ m and $z = 1$ m. We chose results for K_s and θ_s as illustrations for the changing information content. These two parameters are chosen to represent the cross-correlation variation for both saturated and unsaturated parameters.

For the observation point at $x = 106$ m, $y = 100$ m, and $z = 4$ m, as shown in Figure 32.3a at early times, drawdown due to pumping barely reaches the observation location. Most of the water contributing to the pumping wells is from aquifer compaction and water expansion. Observation data are negatively correlated with K_s in the small region between the pumping well and the observation point. At this period, there is negligible amount of water from the drainage of unsaturated zone; therefore, the correlation between head and θ_s is almost zero, which is not shown here.

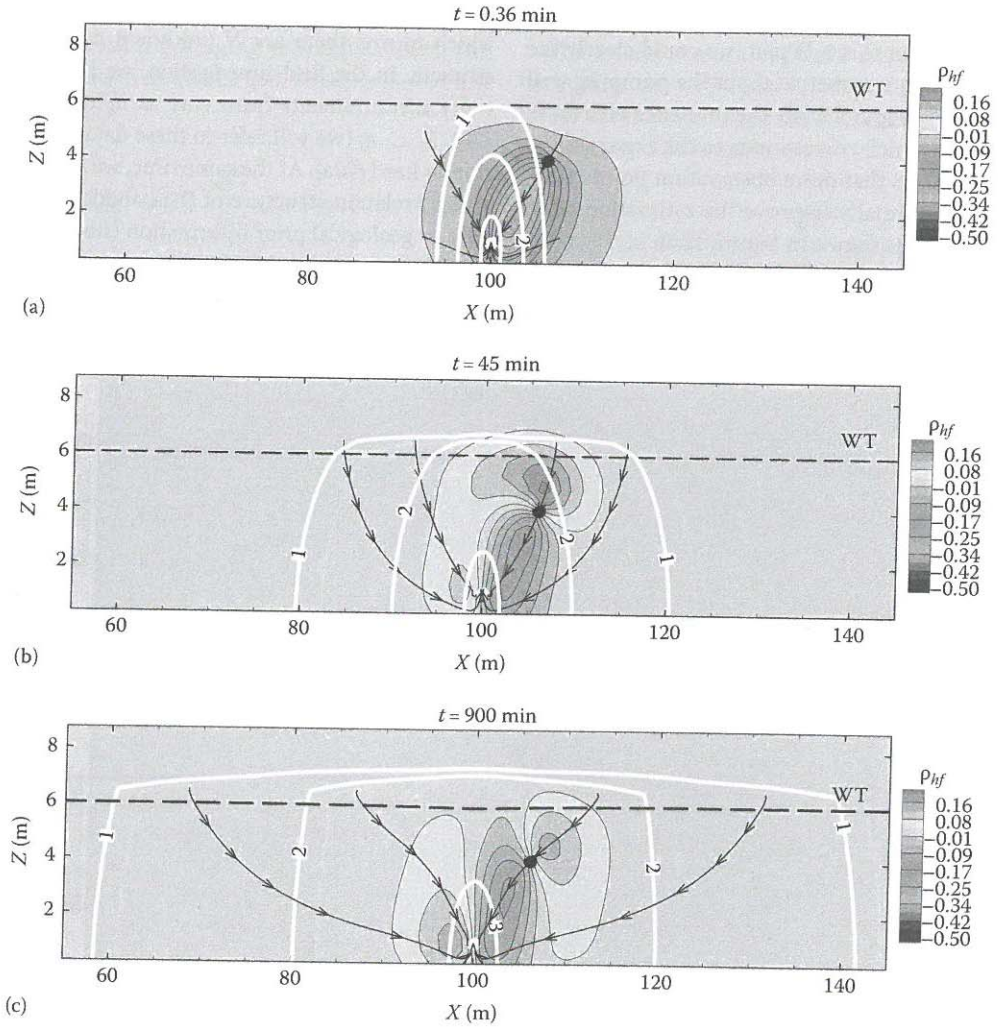

FIGURE 32.3 Cross-correlation between observed heads at $x = 106$ m, $y = 100$ m, and $z = 4$ m (black solid points) and K_s field at three different periods (a) $t = 0.36$, (b) $t = 45$ min, and (c) $t = 900$ min in a cross-sectional view. The cross section goes through $y = 100$ m and the pumping well (white solid point) locates at $x = 100$ m, $y = 100$ m, and $z = 1$ m. The dashed line shows the location of water table (WT) at the same time. Four black lines with arrows are the streamlines and the three white solid lines are the drawdown contours with the values 0.001, 0.012, and 0.15 m. z-axis is exaggerated for illustration. (From Mao, D. et al., *Water Resour. Res.*, 49, 713, 2013a, Figures 2b, 4b and 7b.)

In Figure 32.3b, pumping continues, and cone of depression has already passed the observation location. Head observation correlates with parameters in larger regions. The negative correlation regions become smaller and two positive correlation regions formed. One is in the upstream of the observation location and the other region is on the opposite side of the pumping well. At the same period for the relation with θ_s as indicated in Figure 32.4a, there is only a small correlation region at the vicinity of water table. The small region represents the starting drainage from the unsaturated zone. Positive correlation means larger saturated water content could supply more water to the pumping well, which will maintain a higher observed head in the observation well.

At late times indicated by Figure 32.3c for K_s, the cone of depression expands greatly in lateral directions. Horizontal flow becomes dominant. At this period, most of the water flowing in the pumping well originates from the drainage of the vadose zone. The positive correlated region splits into two regions and expands to large influence areas. A corresponding 3-D plot is shown in Figure 32.5a. From this 3-D plot, we could clearly see that cross-correlation is not symmetric about the pumping well even though the flow is. In Figure 32.4b, the influence area for θ_s expands to a larger area, which corresponds to the expansion of cone of depression. It shows that more observation points from these periods could substantially improve the estimation of θ_s. Its corresponding 3-D plot is shown in Figure 32.5b.

These temporal and spatial variations in cross-correlation contour maps indicate the information content embedded in each observation data. This analysis could help us choose reasonable number of data points during inversion and it also justifies the robustness of HT test than a conventional analytical type curve analysis.

32.5 Successive Linear Estimator

The theory of HT method is explained based on steady-state flow in a confined aquifer. It is then expanded with the addition of transient condition and unsaturated flow. We systematically describe the necessary step for SLE (Yeh et al., 1995, 1996), which is developed by Yeh's research group, and it is the heart for interpreting the data in HT tests.

32.5.1 Steady-State Flow in Confined Aquifers

Suppose the simulation domain is discretized into N blocks, which means there are N unknown hydraulic conductivity to estimate. In the field investigation, we have collected n_f conductivity measurements from core samples, $f_i^* = \ln K_i^* - \overline{f}$, where $i = 1, 2, \ldots, n_f$ (we will refer to these datasets as primary information or hard data). At the same time, we have estimated the mean and correlation structure of the conductivity field based on the data or geological prior information (stochastic representation in Section 32.3). Also assume that during a tomographic pumping test we have collected m sets of n_h observation head values ϕ_j^*, where

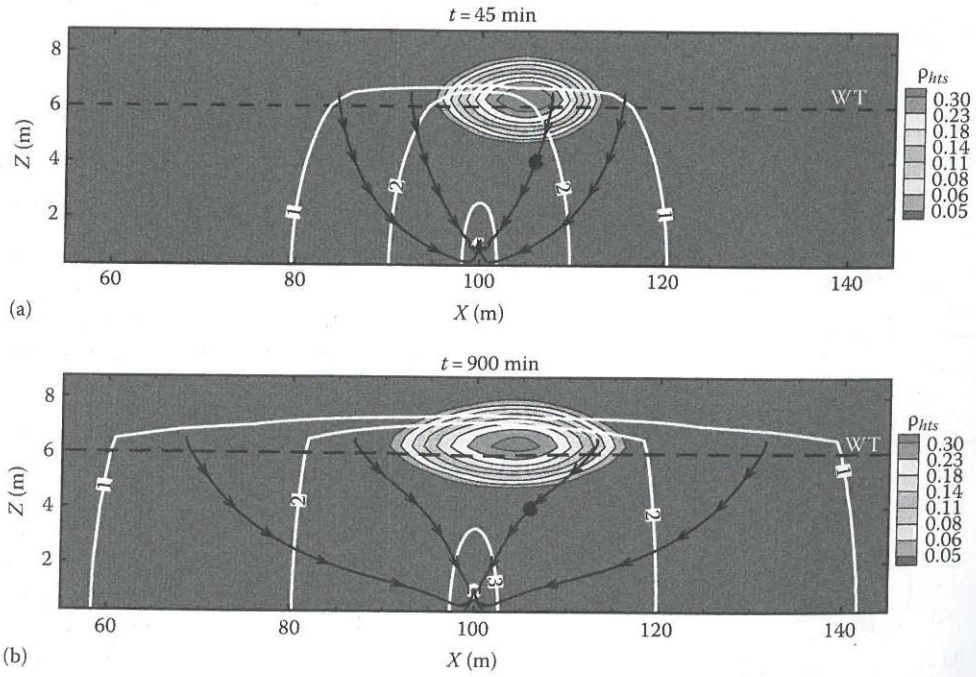

FIGURE 32.4 Cross-correlation between observed heads at $x = 106$ m, $y = 100$ m, and $z = 4$ m (black solid points) and θ_s field at two different periods (a) $t = 45$ min and (b) $t = 900$ min in a cross-sectional view. The cross section goes through $y = 100$ m and the pumping well (white solid point) locates at $x = 100$ m, $y = 100$ m, and $z = 1$ m. The dashed line shows the location of water table (WT) at the same time. Four black lines with arrows are the streamlines and the three white solid lines are the drawdown contours with the values 0.001, 0.012, and 0.15 m. z-axis is exaggerated for illustration. (From Mao, D. et al., *Water Resour. Res.*, 49, 713, 2013a, Figures 6b and 9b.)

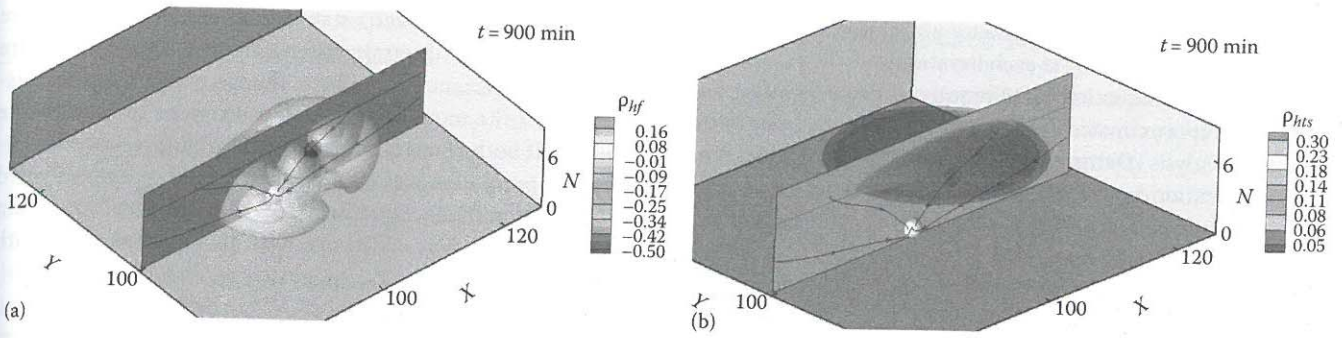

FIGURE 32.5 Cross-correlation 3-D isosurface at late time for the parameter (a) K_s and (b) θ_s. These two figures are corresponding to the 3-D contour map shown by Figures 32.3c and 32.4b. The white solid points represent the pumping wells and observation point is illustrated by the black points. (From Mao, D. et al., *Water Resour. Res.*, 49, 713, 2013a, Figure 10b and d.)

$j = n_f + 1, n_f + 2, \ldots, n_f + mn_h$ during m sequential pumping tests. These head datasets are referred to as secondary information and there is mn_h number of observation data in total.

HT starts with the classical cokriging techniques using the observed f_i^* and h_j^* to construct a cokriged, mean-removed log conductivity map:

$$f_k(\mathbf{x}_0) = \sum_{l=1}^{n_f} \lambda_{l0} f_l^*(\mathbf{x}_l) + \sum_{j=n_f+1}^{n_f+mn_h} \mu_{j0} h_j^*(\mathbf{x}_j) \tag{32.17}$$

where $f_k(\mathbf{x}_0)$ is the cokriged f values at location $\mathbf{x}_0$. Here, λ_{l0} and μ_{j0} are the cokriging weights associated with $\mathbf{x}_0$, which can be evaluated as follows:

$$\begin{aligned}
&\sum_{l=1}^{n_f} \lambda_{l0} R_{ff}(\mathbf{x}_i, \mathbf{x}_l) + \sum_{l=n_f+1}^{n_f+mn_h} \mu_{l0} R_{fh}(\mathbf{x}_i, \mathbf{x}_l) = R_{ff}(\mathbf{x}_0, \mathbf{x}_i) \\
&\quad i = 1, 2, \ldots, n_f \\
&\sum_{l=1}^{n_f} \lambda_{l0} R_{hf}(\mathbf{x}_i, \mathbf{x}_l) + \sum_{l=n_f+1}^{n_f+mn_h} \mu_{l0} R_{hh}(\mathbf{x}_i, \mathbf{x}_l) = R_{hf}(\mathbf{x}_0, \mathbf{x}_i) \\
&\quad i = n_f + 1, n_f + 2, \ldots, n_f + mn_f
\end{aligned} \tag{32.18}$$

where R_{ff}, R_{hh}, and R_{hf} are covariances of f and h and the cross-covariance between f and h. The covariance R_{hh} and the cross-covariance R_{fh} in Equation 32.18 are derived based on first-order numerical approximation, which will be discussed in Equations 32.21 through 32.23.

If there are more than one pumping tests ($m > 1$) during a tomographic test, the observed head data ϕ_j^* can be incorporated either sequentially or simultaneously into the estimation process. At the early stage of computational science, because of the memory issues and computational power limitation, a sequential method is normally used. Different sequences of incorporating pumping tests may produce slightly different parameters distribution (Illman et al., 2009) because of the nonlinear governing equations. In this chapter, we describe the algorithm by incorporating all the test data simultaneously. mn_h data are all used during the cokriging stage in Equation 32.17. Sequential example could refer to Zhu and Yeh (2005).

The information of hydraulic head may not be fully utilized because of the nonlinear relationship between f and h and the linear assumption embedded in cokriging. To circumvent this problem, an SLE is used:

$$Y_c^{(r+1)}(\mathbf{x}_0) = Y_c^{(r)}(\mathbf{x}_0) + \sum_{j=n_f+1}^{n_f+mn_h} \omega_{j0}^{(r)} \left[\phi_j^*(\mathbf{x}_j) - \phi_j^{(r)}(\mathbf{x}_j) \right] \tag{32.19}$$

where

ω_{j0} is the weighting coefficient for the estimate at location $\mathbf{x}_0$ with respect to the head measurement at location $\mathbf{x}_j$

r is the iteration index

$Y_c^{(0)}$ is an estimate of the conditional mean of ln K, which is equal to the cokriged log conductivity field $f_k + \bar{f}$ at $r = 0$. The residual about the mean estimate at an iteration r is $y^{(r)}$. In Equation 32.19, $\phi_j^{(r)}$ is the head at the jth location and ϕ_j^* is the observed head at location j. The values of ω are determined by solving the following system of equations:

$$\begin{aligned}
&\sum_{l=n_f+1}^{n_f+mn_f} \omega_{j0}^{(r)} \varepsilon_{hh}^{(r)}(\mathbf{x}_i, \mathbf{x}_l) + \eta \delta_{ii} = \varepsilon_{hy}^{(r)}(\mathbf{x}_0, \mathbf{x}_i) \\
&\quad i = n_f + 1, n_f + 2, \ldots, n_f + mn_f
\end{aligned} \tag{32.20}$$

where

ε_{hh} and ε_{hy} are the error covariance and error cross-covariance at each iteration

η is a stabilizing term

δ_{ii} is an identity matrix

During the iteration the stabilizing term is added to the diagonal terms of the left-hand-side matrix of 32.20 to numerically condition the matrix and thus to assure a stable solution. In our approach, this stabilizing term is determined dynamically as the

product of a constant weighting factor and the maximum value of the diagonal terms of ε_{hh} at each iteration.

The solution to Equation 32.20 requires knowledge of ε_{hy} and ε_{hh}, which is approximated at each iteration. On the basis of the first-order analysis (Dettinger and Wilson, 1981), hydraulic head at the rth iteration can be written as a first-order Taylor series:

$$\phi = \overline{H}_c^{(r)} + h^{(r)} = G_1(Y_c^{(r)} + f^{(r)}) \approx G_1(Y_c^{(r)}) + \left.\frac{\partial G_1(Y_c^{(r)})}{\partial \ln K}\right|_{Y_c^{(r)}} f^{(r)} \quad (32.21)$$

where G_1 represents the steady-state governing equation 32.1. $\overline{H}_c$ is the conditioned mean head. The first-order approximation of the residual $h^{(r)}$ can then be written as

$$h^{(r)} = \left.\frac{\partial G_1(Y_c^{(r)})}{\partial \ln K}\right|_{\hat{Y}_c^{(r)}} f^{(r)} = J_f^{(r)} f^{(r)} \quad (32.22)$$

We then derived the approximate covariance of $h^{(r)}$ and cross-covariance between $f^{(r)}$ and $h^{(r)}$ in the following two equations:

$$\begin{aligned} \varepsilon_{hh}^{(r)} &= J_f^{(r)} \varepsilon_{ff}^{(r)} J_f^{T(r)} \\ \varepsilon_{hf}^{(r)} &= J_f^{(r)} \varepsilon_{ff}^{(r)} \end{aligned} \quad (32.23)$$

where J_f is the sensitivity matrix with the dimension $mn_h \times N$. It can be evaluated using an adjoint-state method (see Section 32.6 for details). Superscript T stands for the transpose, and ε_{ff} is the covariance of f, which is given by

$$\varepsilon_{ff}^{(1)}(\mathbf{x}_0, \mathbf{x}_k) = R_{ff}(\mathbf{x}_0, \mathbf{x}_k) - \sum_{i=1}^{nf} \lambda_{i0} R_{ff}(\mathbf{x}_i, \mathbf{x}_k) - \sum_{l=1}^{nf+mn_h} \mu_{l0} R_{fh}(\mathbf{x}_l, \mathbf{x}_k) \quad (32.24)$$

At iteration $r = 0$, where $k = 1, 2, \ldots, N$, and λ and μ are the cokriging coefficients. Equation 32.22 is the cokriging variance if $\mathbf{x}_0 = \mathbf{x}_k$. For $r \geq 1$ the covariance are evaluated according to

$$\varepsilon_{ff}^{(r+1)}(\mathbf{x}_0, \mathbf{x}_k) = \varepsilon_{ff}^{(r)}(\mathbf{x}_0, \mathbf{x}_k) - \sum_{l=n_f+1}^{nf+mn_h} \omega_{l0}^{(r)} \varepsilon_{fh}^{(r)}(\mathbf{x}_l, \mathbf{x}_k) \quad (32.25)$$

The covariance is the approximated conditional covariance. The diagonal terms of the covariance matrix is the variance of the parameter at a specific location. During the parameter estimation process, this variance can also be plotted as an indication of the uncertainty from the observation data. Usually, this variance from the last iteration or residual variance is shown in the form of contour maps to represent the reduction of uncertainty for each parameter.

After updating $Y_c(\mathbf{x})$ from Equation 32.19, the governing equation 32.1 is solved again to obtain a newly updated head field ϕ. Equations 32.17 through 32.25 form the necessary steps to implement HT under steady-state conditions. All the steps are kept on iterating until certain criteria are met. These criteria are the change of variance σ_f^2 and the change of biggest head misfit among all the monitoring locations between two successive iterations. If both changes are smaller than the prescribed tolerances, the iteration process stops. If not, ε_{hf} and ε_{hh} are evaluated using Equation 32.23. Equation 32.20 is then solved to obtain a new set of weights, which are used in Equation 32.19 with $\left(\phi_j^* - \phi_j^{(r)}\right)$ to obtain a new estimate of $Y_c(\mathbf{x})$.

32.5.2 Transient-State Flow in Confined Aquifers

During pumping tests, steady state is hardly reached. Head observations always show variation because of storage effect. The equations mentioned earlier need a few changes to adapt transient conditions, which could be described by governing equation 32.2.

If storage measurements from core samples are available, cokriging steps as shown in Equation 32.17 are also performed to produce the parameter distribution. The update of parameters like Equation 32.19 should also be conducted for specific storage separately. For the first-order expansion step, an observed mean head is expanded as

$$\phi \approx G_2\left(Y_c^{(r)}, S_c^{(r)}\right) + \left.\frac{\partial G_2\left(Y_c^{(r)}, S_c^{(r)}\right)}{\partial \ln K}\right|_{Y_c^{(r)}, S_c^{(r)}} f^{(r)} + \left.\frac{\partial G_2\left(Y_c^{(r)}, S_c^{(r)}\right)}{\partial \ln S_s}\right|_{Y_c^{(r)}, S_c^{(r)}} s^{(r)} \quad (32.26)$$

where G_2 represents transient groundwater governing Equation 32.2. S_c is the conditional estimation of $\ln S_s$ at iteration r, and s is the perturbation with respect to the conditional mean. After removing the mean head from Equation 32.26, we have

$$h^{(r)} = J_f^{(r)} f^{(r)} + J_s^{(r)} s^{(r)} \quad (32.27)$$

For the derivation of covariance of $h^{(r)}$ and cross-covariance between $f^{(r)}$, $s^{(r)}$, and $h^{(r)}$ as done in Equation 32.23, we do not consider the correlation between K and S_s. The results are

$$\begin{aligned} \varepsilon_{hh}^{(r)} &= J_f^{(r)} \varepsilon_{ff}^{(r)} J_f^{T(r)} + J_s^{(r)} \varepsilon_{ss}^{(r)} J_s^{T(r)} \\ \varepsilon_{hf}^{(r)} &= J_f^{(r)} \varepsilon_{ff}^{(r)} \\ \varepsilon_{hs}^{(r)} &= J_s^{(r)} \varepsilon_{ss}^{(r)} \end{aligned} \quad (32.28)$$

ε_{ss} is the residual covariance for $\ln S_s$ at iteration r, and it is updated with a similar equation as 32.24 or 32.25. When $r = 0$, it is the initial covariance function and it can be calculated based on autocovariance function, that is, Equation 32.12. If there is not enough information to obtain a covariance function for specific storage, it is usually assumed that it has the same stochastic structure as the hydraulic conductivity.

Different from steady-state condition, there is more than one head observation (secondary data) in the drawdown curve for each observation well. Only a few data points on each drawdown curve are picked for parameter estimation because there is some redundant information among data at different time periods as described by the cross-correlation analysis in Section 32.4 and also more data points require more computation power. A typical choice is 2 data points at early rising limb of the drawdown curve and 2 more data points at the late limb of the drawdown curve. Drawdown data at early period is good for the estimation of S_s and late time data will produce good K_s estimation. This choice is consistent with the cross-correlation pattern between hydraulic parameters and head perturbation.

32.5.3 Transient-State Flow in Unconfined Aquifers

For groundwater flow in unconfined aquifers, we have more hydraulic parameters involved K_s, S_s, a, and θ_s. Each hydraulic parameter has to be stochastically represented as shown by Equations 32.9 and 32.13.

All of these parameters have to be estimated following the procedures as done in steady-state confined aquifers. However, during the first-order approximation step, all of these parameters have to be included in the expansion

$$h^{(r)} = J_f^{(r)} f^{(r)} + J_s^{(r)} s^{(r)} + J_a^{(r)} a^{(r)} + J_{t_s}^{(r)} t_s^{(r)} \tag{32.29}$$

Similar to the calculation for transient condition, the correlation among all the hydraulic parameters are ignored. The corresponding cross-covariance and head covariance can be calculated:

$$\begin{aligned} \varepsilon_{hh} &= J_f \varepsilon_{ff} J_f^T + J_s \varepsilon_{ss} J_s^T + J_a \varepsilon_{aa} J_a^T + J_{t_s} \varepsilon_{t_s t_s} J_{t_s}^T \\ \varepsilon_{hf} &= J_f \varepsilon_{ff} \quad \varepsilon_{hs} = J_s \varepsilon_{ss} \\ \varepsilon_{ha} &= J_a \varepsilon_{aa} \quad \varepsilon_{ht_s} = J_{t_s} \varepsilon_{t_s t_s} \end{aligned} \tag{32.30}$$

The initial estimation of covariance for all the parameters could be based on the core samples. If not available, they can be assigned based on empirical data. Normally, unsaturated parameters have smaller variability, and therefore a smaller variance value could be assigned.

With the inclusion of more parameters for estimation, on each drawdown curve, we need to choose more data points in order to obtain a good estimation. Similar to the data choice for transient flow under saturated condition, we normally add two more data points at late time of the drawdown curve because unsaturated parameters have larger correlation with observation head at this stage. In Section 32.4, we have used saturated water content as an example for the changing cross-correlation of unsaturated parameters.

32.6 Adjoint-State Method

A crucial step during inversion is the evaluation of sensitivity of observed heads with respect to hydraulic parameters. In this content, for each parameter, the sensitivity matrix or Jacobian matrix J will have dimension $N \times mn_d$. N is the number of parameter blocks. mn_d is the total number of observation data during a tomographic test. There is one point we need emphasize that there are often two types of meshes during a numerical implementation of HT method in order to reduce the computation burden. The number N usually represents the number of elements or blocks employed in the parameter estimation step, usually called inversion mesh. It could consist of more than one element or block in order to obtain an accurate numerical result when solving the governing equations or other related equations. The refined mesh is usually called computational mesh.

There are mainly three methods to calculate the sensitivity matrix, perturbation, sensitivity equation, and adjoint-state method. Here, we mainly present the details of adjoint-state method. A brief introduction about other two methods could be found in Yeh (1986).

Adjoint-state method is often employed to obtain sensitivity because of its efficiency. Compared to normal perturbation method, which requires $N+1$ calculation of the forward governing equations, adjoint-state methods only requires solving mn_d times of the adjoint equation plus one time of the forward governing equation, $mn_d \ll N$ under many conditions.

Here, adjoint-state equations for the three flow regimes are given directly without any mathematical derivation. Details can be found in Li and Yeh (1998, 1999), Hughson and Yeh (2000), and Mao et al. (2013a).

$$\nabla \cdot [K(\mathbf{x}) \nabla \Phi] + \delta(\mathbf{x} - \mathbf{x}_k) = 0 \tag{32.31}$$

$$\nabla \cdot [K(\mathbf{x}) \nabla \Phi] + S_s \frac{\partial \Phi}{\partial t} + \delta(\mathbf{x} - \mathbf{x}_p, t - t_c) = 0 \tag{32.32}$$

$$\nabla \cdot [K(\varphi, \mathbf{x}) \nabla \Phi] - \frac{\partial K(\varphi, \mathbf{x})}{\partial \varphi} \nabla \Phi \nabla (\varphi + z) + \left[\beta S_s + C(\varphi, \mathbf{x})\right] \frac{\partial \Phi}{\partial t} + \delta(\mathbf{x} - \mathbf{x}_k, t - t_c) = 0 \tag{32.33}$$

where

Φ is the adjoint variable

$\mathbf{x}_p$ and t_c are the pumping well location vector and time for the observation data

Adjoint-state equations is solved with the following boundary and final time conditions:

$$\begin{aligned} &\Phi = 0 && \text{at } t = t_{final} \\ &\Phi = 0 && \text{at } \Gamma_1 \\ &K(\varphi) \nabla \Phi = 0 && \text{at } \Gamma_2 \end{aligned} \tag{32.34}$$

Equations 32.31 through 32.33 are the adjoint-state equations for steady state and transient state under confined conditions, and transient state under unconfined condition. After solving these equations, several integrations have to be performed to reach the final sensitivity used in the inverse step. Here, we show the integration related to the transient flow in unconfined aquifer. The other two conditions are only simplified versions of the following equations:

$$\frac{\partial h(\mathbf{x}_k,t_c)}{\partial \ln K_s(\mathbf{x}_e)} = \int_T \int_{\Omega_e} -K(\varphi)\nabla\Phi\nabla(\varphi+z)\, d\Omega\, dt \tag{32.35}$$

$$\frac{\partial h(\mathbf{x}_k,t_c)}{\partial \ln \alpha(\mathbf{x}_e)} = \int_T \int_{\Omega_e} \left[-\alpha\frac{\partial K(\varphi)}{\partial \alpha}\nabla\Phi\nabla(\varphi+z) - \alpha\frac{\partial C(\varphi)}{\partial \alpha}\frac{\partial \varphi}{\partial t}\Phi\right] d\Omega\, dt \tag{32.36}$$

$$\frac{\partial h(\mathbf{x}_k,t_c)}{\partial \ln S_S(\mathbf{x}_e)} = \int_T \int_{\Omega_e} -S_S\frac{\partial h}{\partial t}\varphi\Phi\, d\Omega\, dt \tag{32.37}$$

$$\frac{\partial h(\mathbf{x}_k,t_c)}{\partial \ln \theta_S(\mathbf{x}_e)} = \int_T \int_{\Omega_e} -\theta_S\frac{\partial C(\varphi)}{\partial \theta_S}\frac{\partial h}{\partial t}\Phi\, d\Omega\, dt \tag{32.38}$$

During the integration, Ω_e represents the volume of each material element, and it usually is a summation of several computational elements. T is the observation time in the forward sequence.

32.7 Strategy for Implementation of HT Tests

Yeh and Liu (2000) investigated the factors that will affect the design of HT test based on steady state. We summarized their findings as a guide for conducting HT test. In addition, we also add suggestions related to transient data and pumping tests in unconfined aquifer from results of Zhu and Yeh (2005) and Mao et al. (2013a).

1. Horizontal separation distance between observation wells is better set as half of the horizontal correlation. The vertical interval between two pressure monitoring locations should be no more than half of the vertical correlation scale.
2. Optimal number of pumping locations is equal to the ratio of the aquifer depth to the vertical correlation scale.
3. Theoretically, pumping rate has no effect on the estimation. In practice, pressure data may be corrupted by noises. An increase in pumping rate may increase the signal-to-noise ratio such that inversion can yield better results (Illman et al., 2008).
4. Parameter uncertainty in the input variance has no influence on the estimates. Uncertainty in correlation scales has no significant effect on the estimate unless the correlation scales are extremely underestimated or overestimated.
5. To simultaneously estimate hydraulic conductivity and specific storage parameters, head data at both early and late times should be used. Usually 4 or 5 data points from each drawdown curve could be picked for HT inversion. More data points will require more computation power without effectively improving the estimation results.
6. Late time observation data in the unsaturated zone (observation from tensiometer) or near unsaturated zone will improve the estimation unsaturated parameters.

32.8 Examples of HT Tests

HT technique has been verified with many examples as summarized in the introduction. Three cases from literature are chosen to give some details of its application.

32.8.1 Sequential Tomographic Test under Steady-State Conditions

Yeh and Liu (2000) conducted a synthetic test to show the sequential inclusion of pumping test data to improve the estimation of hydraulic conductivity. Even though the theory in Section 32.5 is for simultaneous inclusion of all pumping test data, we feel that it is necessary to present some sequential simulation results to let readers visually see the benefit of conducting a hydraulic tomographic test.

The numerical domain had dimensions 10 m × 5 m × 20 m as shown in Figure 32.6. Five pumping tests were conducted in two vertical boreholes. During each test, 20 pressure measurements were obtained. They also had hydraulic conductivity values at two locations in the domain as conditioning data as these data were available in the field. The pumping tests were operated as steady-state flow.

Figure 32.7b through f shows the estimated hydraulic conductivity with sequential inclusion of data from the five pumping tests. The locations of pumping wells were indicated by the white sphere

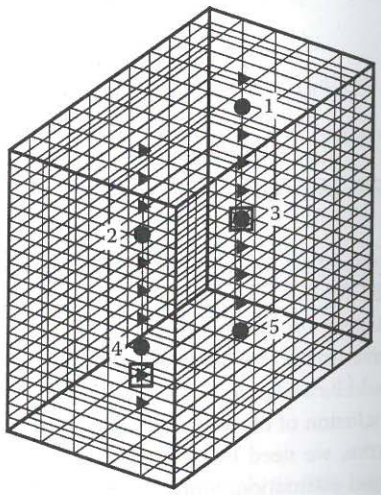

FIGURE 32.6 Schematic map for the hydraulic pumping test conducted in Yeh and Liu (2000). The 20 right triangles are the monitoring locations. The five circles are the pumping locations, and the number represents the sequence of tomographic test. The two squares are the hard data used to conditioned hydraulic conductivity. (From Yeh, T.-C.J. and Liu, S., *Water Resour. Res.*, 36(8), 2095, 2000, Figure 7.)

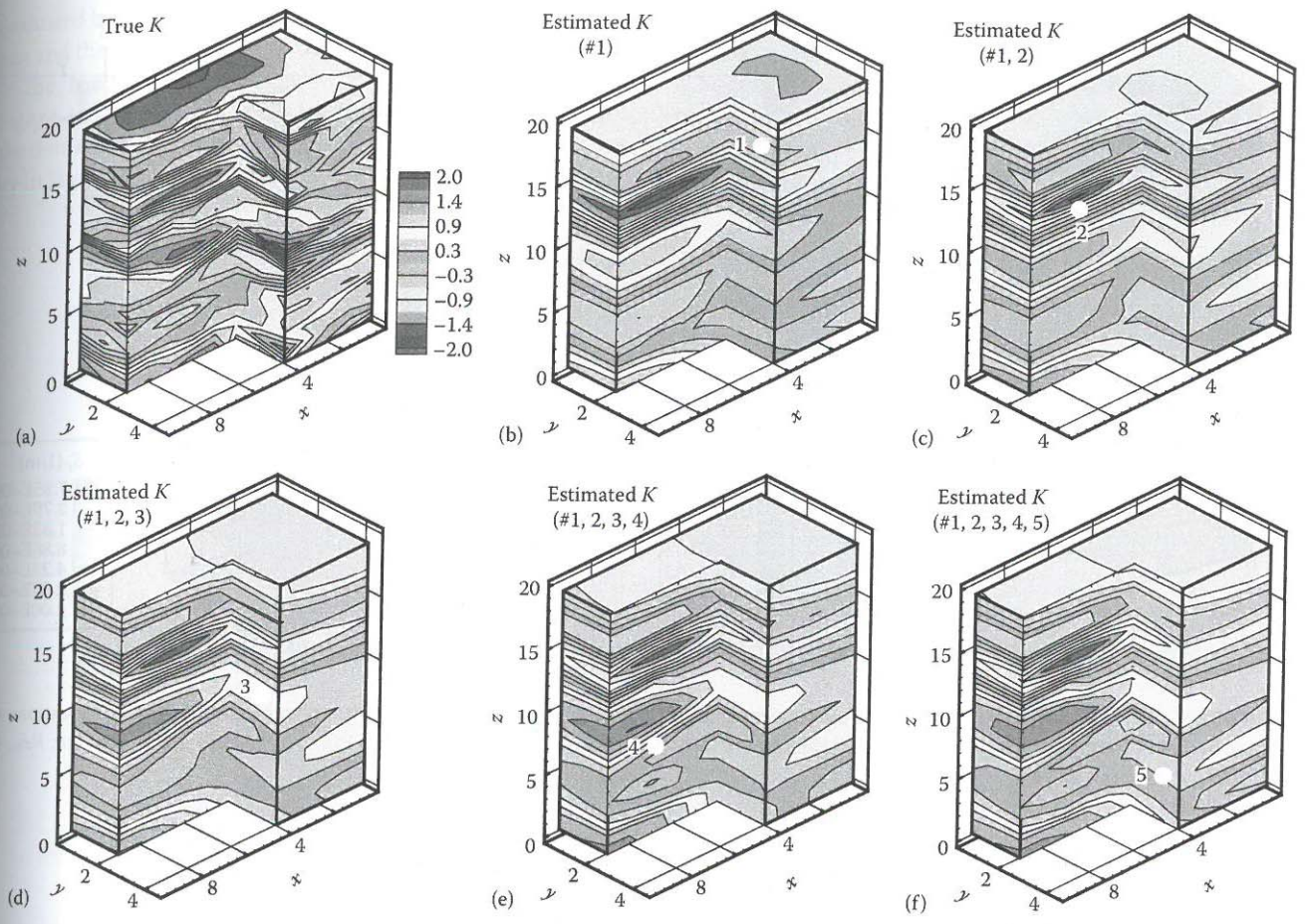

FIGURE 32.7 With sequential inclusion of pumping test conducted at different location indicated by the white sphere from figure (b) through (f). Estimation of hydraulic conductivity reaches the true synthetic field reaches the true synthetic field which is represented by figure (a). (From Yeh, T.-C.J. and Liu, S., *Water Resour. Res.*, 36(8), 2095, 2000, Plate 1.)

in each figure. Compared to the true distribution of hydraulic conductivity in Figure 32.7a, the improvements can be clearly seen from the inclusion of new pumping test data. From the results, we could see that the major features of hydraulic conductivity heterogeneity were already captured after the first test. By including more tests, more details of the heterogeneity were revealed.

32.8.2 Transient Hydraulic Tomography in Fracture Geologic Media

Illman et al. (2009) published some results for a transient HT test conducted in a fractured granite aquifer. Two cross-hole pumping tests were conducted in an underground research laboratory in Japan. There site were characterized by numerous fractures and faults. The purpose of the HT test was to delineate some of the dominant fracture zones.

Two pumping tests were conducted at one of the deep boreholes. The first test was located at intervals of 191–226 m and the second one was at intervals 662–706 m. During each test, several locations were isolated with packers in the boreholes to provide hydraulic pressure measurements.

Figure 32.8 shows their results for the estimated tomograms for hydraulic conductivity and specific storage. HT test captured the high conductivity and low storage zones in the fracture aquifer, which represented fast flow pathways. Those results were also confirmed with the geological data in the same field. These promising results from this research indicated the HT method serve well for delineating large-scale problem.

32.8.3 Hydraulic Tomography Test in a Controlled Sandbox

Estimating heterogeneous hydraulic parameter distribution in unconfined aquifer is quite challenging, while Zhao et al. (2015) conducted sandbox experiments and tried to estimate both saturated and unsaturated parameters simultaneously.

The sandbox used in their experiments was shown in Figure 32.9. Seventeen geological layers were created to simulate the natural environment. Five pumping tests indicated by solid squares were conducted during a HT campaign. During each test, pressure head change during the whole pumping test was monitored in the rest of the ports. Both pressure transducers and

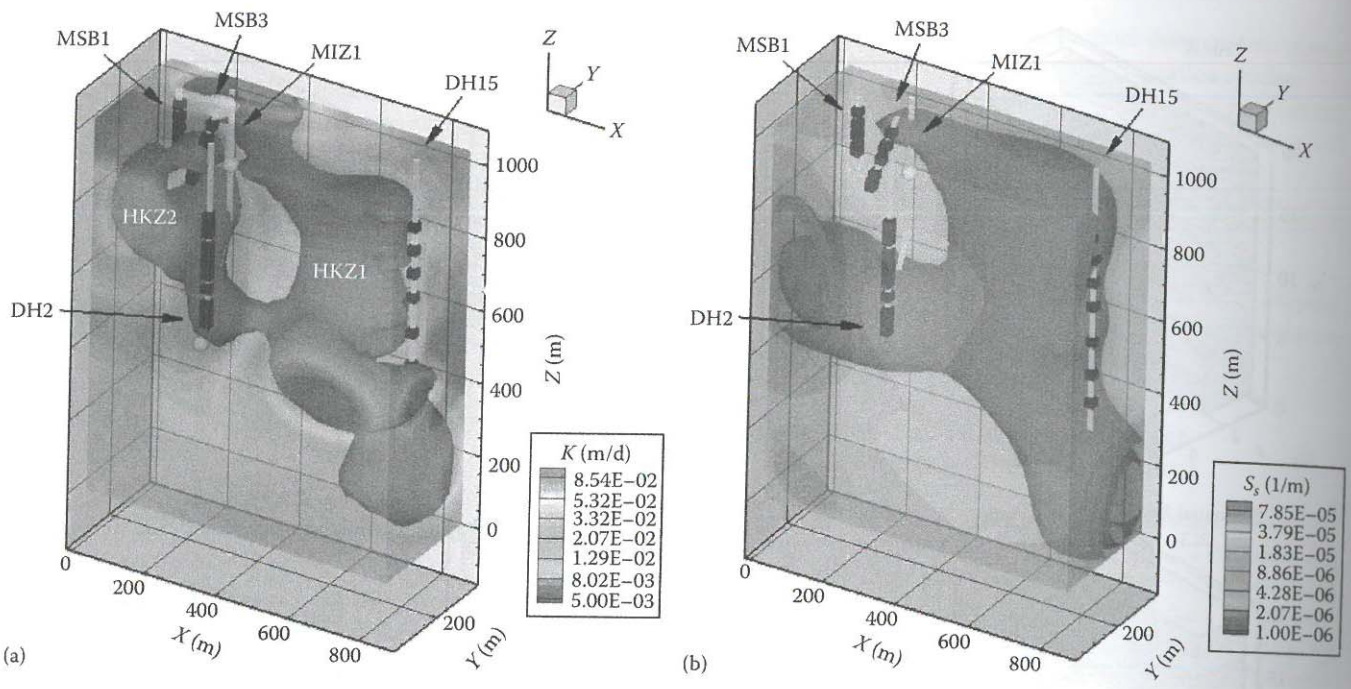

FIGURE 32.8 3-D K tomogram (m/d) (a) and S_s tomograms (1/m) (b) obtained from the inversion of two cross-hole tests. Pumping locations are indicated by solid white spheres, while observation intervals are indicated by solid black squares. (From Illman, W.A. et al., *Water Resour. Res.*, 45, W01406, 2009, Figures 4 and 6.)

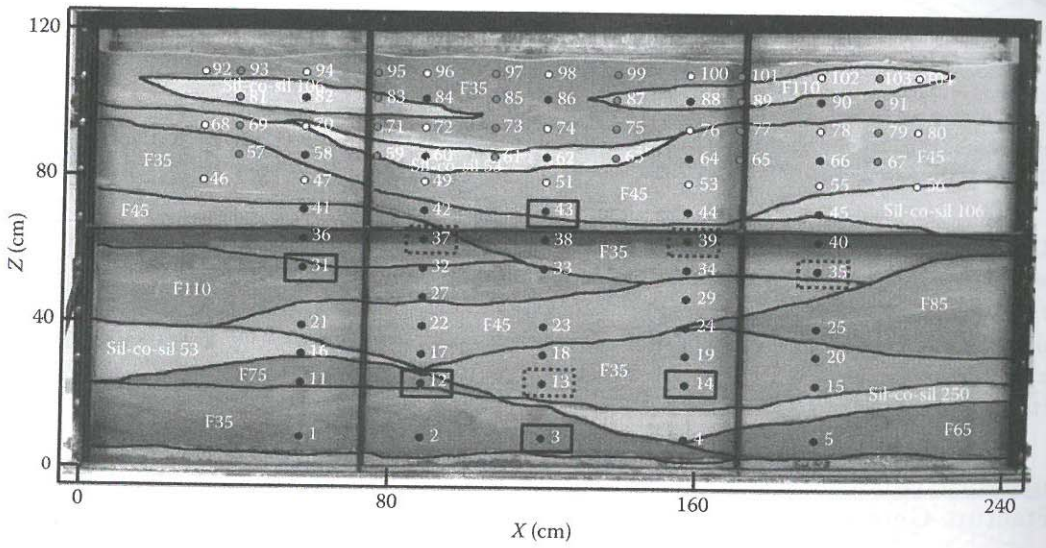

FIGURE 32.9 Front view of sandbox aquifer used for pumping tests showing layers and port locations. Solid black circles indicate the pressure transducer ports; solid white circles indicate the tensiometer ports; solid gray circles indicate the water content sensor ports. Squares indicate the pumped ports to generate the drawdown data for inverse modeling, while the dashed squares are pumped ports to generate data for validation purposes. (From Zhao, Z. et al., *Water Resour. Res.*, 51, 4137, 2015, Figure 1.)

tensiometers were employed to capture the pressure change in saturated and unsaturated zones.

Their estimated results for K_s, S_s, α (pore size parameter in Equation 32.7), and θ_s were shown in Figure 32.10. Results revealed that the HT analysis was able to accurately capture the location and extent of heterogeneity including high and low K_s layers within the saturated and unsaturated zones, as well as the general distribution pattern of α and θ_s for the Gardner–Russo's model in unsaturated flow influenced region, and S_s; we could only have the estimated results in the saturated zone. The estimated tomograms were

evaluated by both visual inspection with stratigraphy in the sandbox and the pumping tests not used for HT tests.

The residual variance for each parameter was shown in Figure 32.11. For K_s the variance had reduction everywhere in the domain, which is indicated by the characterized heterogeneity in Figure 32.10a. As for S_s, the low residual variance on the top of the domain was from numerical errors and we can only trust the results in the saturated zone. Unsaturated parameters α and θ_s both had a reasonable reduction of uncertainty in the unsaturated zone and the residual variance were almost constant in the saturated zone, which indicated the limited influence of unsaturated flow to the saturated zone.

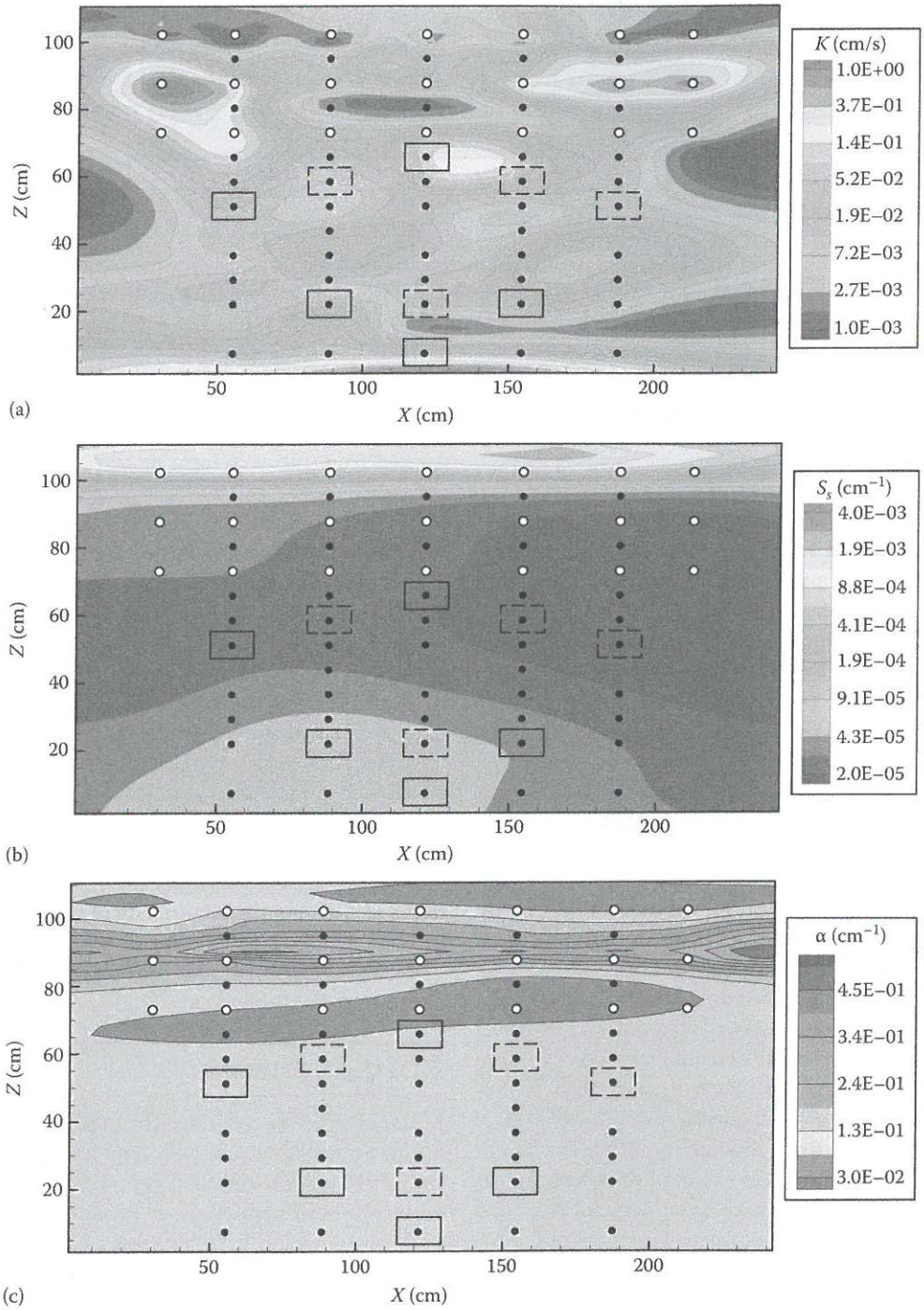

FIGURE 32.10 Estimated tomograms of (a) K, (b) S_s using sandbox pumping test data. Solid squares indicate the pumping ports used for inverse estimation. Dashed squares indicate the pumping ports used for validation purposes. ● indicates locations for pressure transducers. ○ indicates locations for tensiometers. (From Zhao, Z. et al., *Water Resour. Res.*, 51, 4137, 2015, Figure 2.) (c) α *(Continued)*

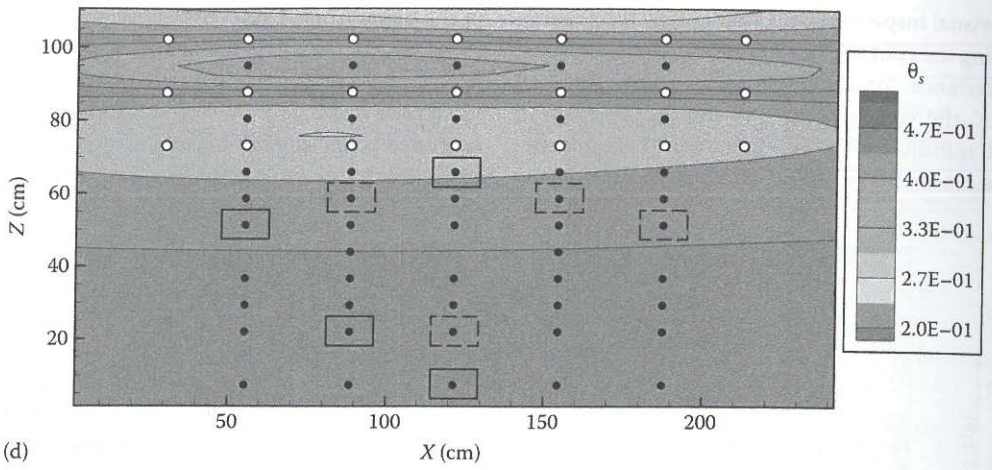

FIGURE 32.10 (*Continued*) Estimated tomograms of (d) θ_s using sandbox pumping test data. Solid squares indicate the pumping ports used for inverse estimation. Dashed squares indicate the pumping ports used for validation purposes. ● indicates locations for pressure transducers. ○ indicates locations for tensiometers. (From Zhao, Z. et al., *Water Resour. Res.*, 51, 4137, 2015, Figure 2.)

32.9 Tomographic Tests in Geophysics

Geophysical imaging allows the nonintrusive imaging of petrophysical properties. Methods are typically categorized as active (using sources and receivers, e.g., georadar and seismic) or passive with only a set of receivers (self-potential and gravity). Geophysical information can also be used to supply further information to hydraulic tomography. One approach is to use cokriging or kriging with external drift if the petrophysical property derived from geophysical tomography show some degree of correlation with the hydraulic properties (for instance, Troisi et al., 2000). Along these lines, we can note that some petrophysical properties imaged using an active method named induced polarization shows some strong correlation with hydraulic conductivity (see Revil and Florsch, 2010). In addition, active and passive methods can be used to monitor pumping tests because of their direct sensitivity to hydraulic parameters. In gravity, we measured the vertical acceleration of the gravity field at the ground surface. These gravity measurements can be used to probe the mass density of the subsurface. Time-lapse gravity measurements can be used to image changes in the water content during pumping tests (e.g., Gonzales-Quiros and Fernandez-Alvarez, 2014). The self-potential method is another passive geophysical technique in which the electrical field is passively measured at the ground surface using a network of electrodes and a voltmeter (Revil and Jardani, 2013). The flow of water in a porous material drags the excess of electrical charges contained in the vicinity of the pore water mineral interface, creating a tiny electrical current of electrokinetic nature. Self-potential measurements can also be used directly to assess the distribution of the Darcy velocity and the hydraulic conductivity of confined aquifers (see Soued Ahmed et al., 2014).

Various studies clearly illustrates that petrophysical properties derived from geophysical imaging (e.g., p-wave velocity derived from full waveform or travel time tomography) does not correlate very well with the hydraulic properties estimated by HT (e.g., Brauchler et al., 2012). However, despite that the distribution of these properties are different from the distribution of the hydraulic parameters, we can expect that such geophysical survey can yield the shape or boundary of the hydraulic conductivity distribution. Indeed, both surveys may be used to derive a similar geostatistical structure (in a statistic sense). For instance, the structural information existing in migrated seismic and georadar migrated images can be used to guide the inversion of the hydraulic data using an approach called image-guided inversion (see Zhou et al., 2014; Soued Ahmed et al., 2015).

There are many different ways to couple geophysical and hydrogeological information together, the most efficient in terms of reducing the non-unicity of the inverse problem being through a fully coupled joint inversion (for instance, Jardani et al., 2013). A review of recent developments in hydrogeophysics can be found in Binley et al. (2015).

32.10 Summary

In this chapter, we described the newly developed aquifer characterization method hydraulic tomography. We started from the statistic basement, and then gave the detailed theoretical background for steady and transient conditions. Three examples were given to illustrate the robustness of this new technique. Our intent was not to cover all the research on this topic but rather to provide mathematical background behind this technique and some examples to prove the robustness of this new technology.

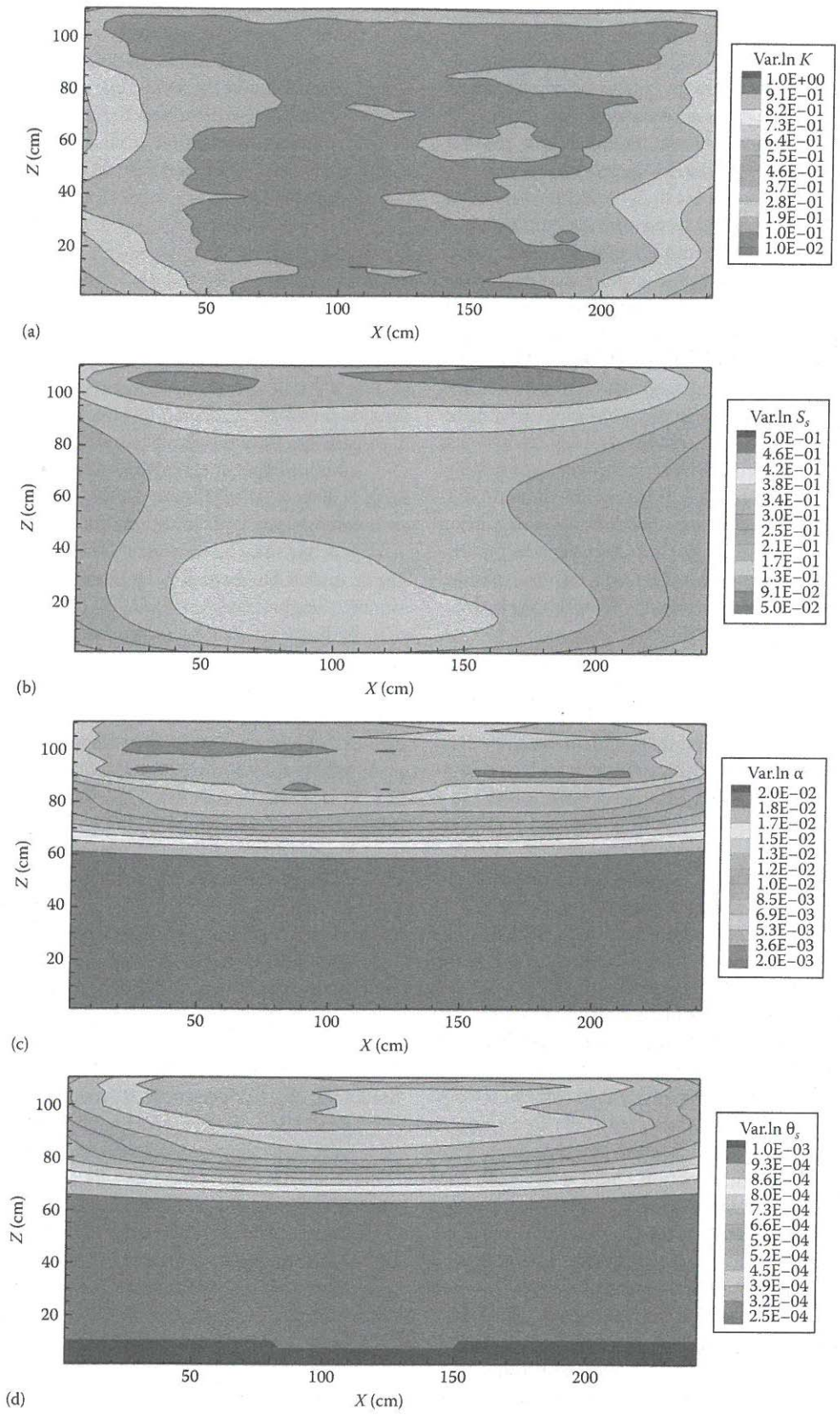

FIGURE 32.11 Residual variance of estimated tomograms for (a) ln K, (b) ln S_s, (c) ln α, and (d) ln θ_s. (From Zhao, Z. et al., *Water Resour. Res.*, 51, 4137, 2015, Figure 4.)

Glossary

Adjoint-state method: A numerical method for efficiently computing the sensitivity of a function (gradient of a function). The number of equations it solves only depends on the number of observation data not the number of unknowns.

Cokriging: Cokriging is a geostatistical technique used for interpolation purpose. It is a linear-weighted averaging method, and its weight depends not only on distance but also on the direction and orientation of the neighboring data to the unsampled location. Different from Kriging interpolation method that uses relation of only one variable at different locations, it takes advantages of the relation between two or more variables.

Cross-correlation: The relation between a system response and system parameter. In the hydraulic tomography background, it is used to represent the relationship between an observed head with the hydraulic parameters everywhere in the domain. It ranges between –1.0 and 1.0.

First-order approximation: A truncated Taylor series expansion in which only the first-order terms are kept. In the current content, hydraulic head perturbation is expanded with only first-order terms from the unknown hydraulic parameters.

Hydraulic tomography: An aquifer is stressed by pumping water from or injecting water into a well, and the response is monitored at other wells. A set of stresses/responses yields independent sets of data. Sequentially switching the pumping or injection locations, without installing additional wells, results in a large number of aquifer response caused by stress at different locations.

Material mesh: A type of mesh used for assigning material value, that is, the value of hydraulic conductivity, to a specific element of a numerical model. Usually the value is constant in one material element. Each material element could be further refined with smaller elements, which are used for numerical computation, that is, finite element method. The refined mesh is usually called computation mesh.

Primary information: It is also known as hard data, which represents the information collected from core samples. It could be a hydraulic conductivity, saturated water content, etc. The information could be directly used in a parameter estimation process and these values are fixed during estimation process.

Secondary information: Data collected during a tomographic test, that is, hydraulic head measurements. The data are used in the estimation process to update unknown parameter field.

Sensitivity: The response of a hydraulic head with respect to a hydraulic parameter, that is, hydraulic conductivity. For parameter estimation, we usually use the response of a hydraulic head with respect to the logarithm of a hydraulic parameter in order to avoid negative value.

Simultaneous hydraulic tomography: A different data assimilation method compared to "sequential hydraulic tomography." All the observed secondary information is utilized at the same time during parameter estimation process. In sequential hydraulic tomography, secondary information from different pumping tests is used one after one during the parameter estimation process.

References

Berg, S. J. and W. A. Illman (2011a), Three-dimensional transient hydraulic tomography in a highly heterogeneous glaciofluvial aquifer-aquitard system, *Water Resour Res, 47*, W10507.

Berg, S. J. and W. A. Illman (2011b), Capturing aquifer heterogeneity: Comparison of approaches through controlled sandbox experiments, *Water Resour Res, 47*(9), W09514.

Berg, S. J. and W. A. Illman (2015), Comparison of hydraulic tomography with traditional methods at a highly heterogeneous site, *Groundwater, 53*, 71–89.

Binley, A., S. S. Hubbard, J. A. Huisman, A. Revil, D. A. Robinson, K. Singha, and L. D. Slater (2015), The emergence of hydrogeophysics for improved understanding of subsurface processes over multiple scales, *Water Resour Res, 51*, 3837–3866.

Bohling, G. C., J. J. Butler, Jr., X. Zhan, and M. D. Knoll (2007), A field assessment of the value of steady shape hydraulic tomography for characterization of aquifer heterogeneities, *Water Resour Res, 43*(5), W05430.

Bohling, G. C., X. Zhan, J. J. Butler, Jr., and L. Zheng (2002), Steady shape analysis of tomographic pumping tests for characterization of aquifer heterogeneities, *Water Resour Res, 38*(12), 1324.

Boulton, N. S. (1963), Analysis of data from non-equilibrium pumping tests allowing for delayed yield from storage, *Proceedings of the Institution of Civil Engineers, 26*(3), 469–482.

Brauchler, R., G. Böhm, C. Leven, P. Dietrich, and M. Sauter (2013), A laboratory study of tracer tomography, *Hydrogeol J, 21*(6), 1265–1274.

Brauchler, R., J. Doetsch, P. Dietrich, and M. Sauter (2012), Derivation of site-specific relationships between hydraulic parameters and p-wave velocities based on hydraulic and seismic tomography, *Water Resour Res, 48*(3), W03531.

Brauchler, R., R. Hu, P. Dietrich, and M. Sauter (2011), A field assessment of high-resolution aquifer characterization based on hydraulic travel time and hydraulic attenuation tomography, *Water Resour Res, 47*(3), W03503.

Brauchler, R., R. Liedl, and P. Dietrich (2003), A travel time based hydraulic tomographic approach, *Water Resour Res, 39*(12), 1370.

Cardiff, M., T. Bakhos, P. K. Kitanidis, and W. Barrash (2013), Aquifer heterogeneity characterization with oscillatory pumping: Sensitivity analysis and imaging potential, *Water Resour Res, 49*, 5395–5410.

Cardiff, M. and W. Barrash (2011), 3-D transient hydraulic tomography in unconfined aquifers with fast drainage response, *Water Resour Res, 47*, W12518.

Castagna, M. and A. Bellin (2009), A Bayesian approach for inversion of hydraulic tomographic data, *Water Resour Res, 45*, W04410.

Cooper, H. H. and C. E. Jacob (1946), A generalized graphical method for evaluating formation constants and summarizing well field history, *Trans Am Geophys Union, 27*, 526–534.

Dagan, G. (1967), A method of determining the permeability and effective porosity of unconfined anisotropie aquifers, *Water Resour Res, 3*(4), 1059–1071.

Dettinger, M. and J. Wilson (1981), First order analysis of uncertainty in numerical models of groundwater flow part 1. Mathematical development, *Water Resour Res, 17*(1), 149–161.

Fienen, M. N., T. Clemo, and P. K. Kitanidis (2008), An interactive Bayesian geostatistical inverse protocol for hydraulic tomography, *Water Resour Res, 44*, W00B01.

Gardner, W. (1958), Some steady-state solutions of the unsaturated moisture flow equation with application to evaporation from a water table, *Soil Sci, 85*(4), 228–232.

González-Quirós, A. and J. Fernández-Álvarez (2014), Simultaneous solving of three-dimensional gravity anomalies caused by pumping tests in unconfined aquifers, *Math Geosci, 46*(6), 649–664.

Hao, Y., T.-C. J. Yeh, J. Xiang, W. A. Illman, K. Ando, K.-C. Hsu, and C.-H. Lee (2008), Hydraulic tomography for detecting fracture zone connectivity, *Ground Water, 46*(2), 183–192.

Huang, S.-Y., J.-C. Wen, T.-C. J. Yeh, W. Lu, H.-L. Juan, C.-M. Tseng, J.-H. Lee, and K.-C. Chang (2011), Robustness of joint interpretation of sequential pumping tests: Numerical and field experiments, *Water Resour Res, 47*, W10530.

Hughson, D. L. and T.-C. J. Yeh (2000), An inverse model for three-dimensional flow in variably saturated porous media, *Water Resour Res, 36*(4), 829–839.

Illman, W. A., S. J. Berg, and T.-C. J. Yeh (2012), Comparison of approaches for predicting solute transport: Sandbox experiments, *Ground Water, 50*(3), 421–431.

Illman, W. A., A. J. Craig, and X. Liu (2008), Practical issues in imaging hydraulic conductivity through hydraulic tomography, *Ground Water, 46*(1), 120–132.

Illman, W. A., X. Liu, S. Takeuchi, T.-C. J. Yeh, K. Ando, and H. Saegusa (2009), Hydraulic tomography in fractured granite: Mizunami Underground Research site, Japan, *Water Resour Res, 45*(1), W01406.

Illman, W. A., X. Y. Liu, and A. Craig (2007), Steady-state hydraulic tomography in a laboratory aquifer with deterministic heterogeneity: Multi-method and multiscale validation of hydraulic conductivity tomograms, *J Hydrol, 341*(3–4), 222–234.

Illman, W. A., J. F. Zhu, A. J. Craig, and D. T. Yin (2010), Comparison of aquifer characterization approaches through steady state groundwater model validation: A controlled laboratory sandbox study, *Water Resour Res, 46*, W04502.

Jardani, A., A. Revil, and J. P. Dupont (2013), Stochastic joint inversion of hydrogeophysical data for salt tracer test monitoring and hydraulic conductivity imaging, *Adv Water Res, 52*, 62–77.

Kitanidis, P. K. (1995), Quasi-linear geostatistical theory for inversing, *Water Resour Res, 31*(10), 2411–2419.

Li, B. and T.-C. J. Yeh (1998), Sensitivity and moment analyses of head in variably saturated regimes, *Adv Water Res, 21*(6), 477–485.

Li, B. and T.-C. J. Yeh (1999), Cokriging estimation of the conductivity field under variably saturated flow conditions, *Water Resour Res, 35*(12), 3663–3674.

Li, W., A. Englert, O. A. Cirpka, J. Vanderborght, and H. Vereecken (2007), Two-dimensional characterization of hydraulic heterogeneity by multiple pumping tests, *Water Resour Res, 43*(4), W04433.

Liu, S., T.-C. J. Yeh, and R. Gardiner (2002), Effectiveness of hydraulic tomography: Sandbox experiments, *Water Resour Res, 38*(4), 1034.

Liu, X., W. A. Illman, A. J. Craig, J. Zhu, and T.-C. J. Yeh (2007), Laboratory sandbox validation of transient hydraulic tomography, *Water Resour Res, 43*(5), W05404.

Liu, X. and P. K. Kitanidis (2011), Large-scale inverse modeling with an application in hydraulic tomography, *Water Resour Res, 47*(2), W02501.

Mao, D., T.-C. J. Yeh, L. Wan, C.-H. Lee, K.-C. Hsu, J.-C. Wen, and W. Lu (2013a), Cross-correlation analysis and information content of observed heads during pumping in unconfined aquifers, *Water Resour Res, 49*(2), 713–731.

Mao, D., T.-C. J. Yeh, L. Wan, J.-C. Wen, W. Lu, C.-H. Lee, and K.-C. Hsu (2013b), Joint interpretation of sequential pumping tests in unconfined aquifers, *Water Resour Res, 49*(4), 1782–1796.

Mathias, S. A. and A. P. Butler (2006), Linearized Richards' equation approach to pumping test analysis in compressible aquifers, *Water Resour Res, 42*, W06408.

Mishra, P. K. and S. P. Neuman (2010), Improved forward and inverse analyses of saturated-unsaturated flow toward a well in a compressible unconfined aquifer, *Water Resour Res, 46*, W07508.

Moench, A. F. (1995), Combining the Neuman and Boulton models for flow to a well in an unconfined aquifer, *Ground Water, 33*(3), 378–384.

Mualem, Y. (1976), A new model for predicting the hydraulic conductivity of unsaturated porous media, *Water Resour Res, 12*(3), 513–522.

Neuman, S. P. (1972), Theory of flow in unconfined aquifers considering delayed response of the water table, *Water Resour Res, 8*(4), 1031–1045.

Ni, C. F. and T. C. J. Yeh (2008), Stochastic inversion of pneumatic cross-hole tests and barometric pressure fluctuations in heterogeneous unsaturated formations, *Adv Water Res, 31*(12), 1708–1718.

Ni, C.-F., T.-C. J. Yeh, and J.-S. Chen (2009), Cost-effective hydraulic tomography surveys for predicting flow and transport in heterogeneous aquifers, *Environ Sci Technol, 43*(10), 3720–3727.

Revil, A. and N. Florsch (2010), Determination of permeability from spectral induced polarization in granular media, *Geophys J Int*, *181*(3), 1480–1498.

Revil, A. and A. Jardani (2013), *The Self-Potential Method: Theory and Applications in Environmental Geosciences*, Cambridge, U.K., Cambridge University Press.

Russo, D. (1988), Determining soil hydraulic properties by parameter estimation: On the selection of a model for the hydraulic properties, *Water Resour Res*, *24*(3), 453–459.

Sharmeen, R., W. A. Illman, S. J. Berg, T.-C. J. Yeh, Y.-J. Park, E. A. Sudicky, and K. Ando (2012), Transient hydraulic tomography in a fractured dolostone: Laboratory rock block experiments, *Water Resour Res*, *48*(10), W10532.

Soueid Ahmed, A., A. Jardani, A. Revil, and J. P. Dupont (2014), Hydraulic conductivity field characterization from the joint inversion of hydraulic heads and self-potential data, *Water Resour Res*, *50*(4), 3502–3522.

Soueid Ahmed, A., J. Zhou, A. Jardani, A. Revil, and J. P. Dupont (2015), Image-guided inversion in steady-state hydraulic tomography, *Adv Water Res*, 82(0), 83–97.

Straface, S., T.-C. J. Yeh, J. Zhu, S. Troisi, and C.-H. Lee (2007), Sequential aquifer tests at a well field, Montalto Uffugo Scalo, Italy, *Water Resour Res*, *43*(7), W07432.

Streltsova, T. D. (1976a), Analysis of aquifer-aquitard flow, *Water Resour Res*, *12*(3), 415–422.

Streltsova, T. D. (1976b), Analysis of pumping test data from anisotropic unconfined aquifers considering delayed gravity response—Reply, *Water Resour Res*, *12*(1), 113–114.

Sudicky, E. (1986), A natural gradient experiment on solute transport in a sand aquifer: Spatial Variability of hydraulic conductivity and its role in the dispersion process, *Water Resour Res*, *22*(13), 2069–2082.

Sun, R., T.-C. J. Yeh, D. Mao, M. Jin, W. Lu, and Y. Hao (2013), A temporal sampling strategy for hydraulic tomography analysis, *Water Resour Res*, *49*(7), 3881–3896.

Theis, C. V. (1935), The relation between the lowering of the piezometric surface and the rate and duration of discharge of a well using ground water storage, *Trans Am Geophys Union*, *16*, 519–514.

Troisi, S., C. Fallico, S. Straface, and E. Migliari (2000), Application of kriging with external drift to estimate hydraulic conductivity from electrical-resistivity data in unconsolidated deposits near Montalto Uffugo, Italy, *Hydrogeol J*, *8*(4), 356–367.

van Genuchten, M. T. (1980), A closed-form equation for predicting the hydraulic conductivity of unsaturated soils, *Soil Sci Soc Am J*, *44*(5), 892–898.

Vasco, D. W. and K. Karasaki (2001), Inversion of pressure observations: An integral formulation, *J Hydrol*, 253(1–4), 27–40.

Wu, C.-M., T.-C. J. Yeh, J. Zhu, T.-H. Lee, N.-S. Hsu, C.-H. Chen, and A. F. Sancho (2005), Traditional analysis of aquifer tests: Comparing apples to oranges, *Water Resour Res*, *41*(9), W09402.

Xiang, J., T.-C. J. Yeh, C.-H. Lee, K.-C. Hsu, and J.-C. Wen (2009), A simultaneous successive linear estimator and a guide for hydraulic tomography analysis, *Water Resour Res*, *45*(2), W02432.

Yeh, T.-C. J., A. L. Gutjahr, and M. Jin (1995), An iterative cokriging-like technique for ground-water flow modeling, *Ground Water*, *33*(1), 33–41.

Yeh, T.-C. J., M. Jin, and S. Hanna (1996), An iterative stochastic inverse method: Conditional effective transmissivity and hydraulic head fields, *Water Resour Res*, *32*(1), 85–92.

Yeh, T.-C. J. and S. Liu (2000), Hydraulic tomography: Development of a new aquifer test method, *Water Resour Res*, *36*(8), 2095–2105.

Yeh, W.-G. (1986), Review of parameter identification procedures in groundwater hydrology: The inverse problem, *Water Resour Res*, *22*(2), 95–108.

Yin, D. T. and W. A. Illman (2009), Hydraulic tomography using temporal moments of drawdown recovery data: A laboratory sandbox study, *Water Resour Res*, *45*, W01502.

Zha, Y., T.-C. J. Yeh, D. Mao, J. Yang, and W. Lu (2014), Usefulness of flux measurements during hydraulic tomographic survey for mapping hydraulic conductivity distribution in a fractured medium, *Adv Water Res*, *71*(0), 162–176.

Zhao, Z., W. A. Illman, T.-C. J. Yeh, S. J. Berg, and D. Mao (2015), Validation of hydraulic tomography in an unconfined aquifer: A controlled sandbox study, *Water Resour Res*, *51*, 4137–4155.

Zhou, J., A. Revil, M. Karaoulis, D. Hale, J. Doetsch, and S. Cuttler (2014), Image-guided inversion of electrical resistivity data, *Geophys J Int*, *197*, 292–309.

Zhu, J. and T.-C. J. Yeh (2005), Characterization of aquifer heterogeneity using transient hydraulic tomography, *Water Resour Res*, *41*, W07028.

Further Information

By far, there are no textbooks on the subject of hydraulic tomography. We choose several references from the literature as further information.Berg and Illman (2014) showed the advantages of conducting HT test in a highly heterogeneous field site with comparison with other traditional aquifer characterization methods.

Illman et al. (2010) and Cardiff and Barrash (2011) could both serve as literature reviews for the development of HT technology.

Kitanidis (1995) and Yeh et al. (1996) could serve as the theoretical support for geostatistically based inverse method with first-order approximation.